Hindawi
International Journal of Antennas and Propagation
Volume 2019, Article ID 3857964, 10 pages
https://doi.org/10.1155/2019/3857964

Research Article

Design of Series-Fed Bandwidth-Enhanced Microstrip Antenna Array for Millimetre-Wave Beamforming Applications

Hung-Chen Chen,[1] **Tsenchieh Chiu**,[1] **and Ching-Luh Hsu**[2]

[1]*National Central University, Taoyuan, Taiwan*
[2]*National Chung-Shan Institute of Science and Technology, Taoyuan, Taiwan*

Correspondence should be addressed to Tsenchieh Chiu; tcchiu@ee.ncu.edu.tw

Received 20 February 2019; Revised 15 April 2019; Accepted 15 May 2019; Published 3 June 2019

Academic Editor: Ikmo Park

A novel series-fed microstrip patch array antenna for 37/39 GHz beamforming is proposed. To improve the antenna bandwidth, two of the patches are modified with truncated corners in the diagonal direction. This truncation generates two degenerate resonances which result in a flattened frequency response of the input impedance. Then, the recessed microstrip feeds for the other two patches are designed to yield a proper current distribution for radiation while maintaining minimal return loss, wide bandwidth, and low sidelobes. Though the individual patch antenna is elliptically polarized due to the truncated corners, a phased array with linear polarization can still be obtained by alternately deploying left-handed and right-handed elliptically polarized patches. For validation of the proposed design, an array is fabricated with 16 elements on a substrate with 10 mil thickness and ε_r =2.2. The beamforming capability of the proposed array is also demonstrated. The experiment results agree well with the simulation and show that the antenna gain and the return loss bandwidth can be more than 21 dBi and 8%, respectively.

1. Introduction

Recent researches have shown that millimetre-wave spectrum is capable of providing the capacity required for future wireless data applications including cellular systems [1, 2], LAN [3], fixed access, and backhaul [4]. In the next generation of the International Mobile Telecommunications (IMT), the millimetre-wave technique has been among one of the key technologies [5]. The Federal Communications Commission (FCC) has taken the initiative to approve the use of several bands in millimetre spectrum for 5G systems [6]. To take advantage of the large bandwidth in millimetre wave, the system gain has to be significantly increased to compensate the severe propagation losses which are intrinsic in this spectrum. Active phased array with beamforming capability is an effective approach to achieve high performance for 5G millimetre-wave systems. The cost to implement an active array, however, may be quite high. Fortunately, the continuous advancement of device technology makes it possible to build such an array cost-effectively [1].

Various types of antenna arrays have been proposed for 28, 37, and 39 GHz systems [7–15]. In [7], a 28-GHz 4×2 circular-polarization microstrip antenna subarray is designed. In [8], a 28-GHz 16-element mesh-grid patch antenna array is realized on a multilayer FR4 with low radiation efficiency. In [9], a switchable phased array composed of three subarrays of patch antennas is proposed for coverage extension. Each subarray can cover ± 40° scanning range by controlling phase shifter assemblies (PSA). In [10], a 28/38 GHz dual-band microstrip printed slot antenna array is proposed. In [11], 2×2 and 3×3 series-fed patch arrays for 28-GHz beam-steering applications are designed. In [12], a 37-GHz dual-polarized 2×2 subarray antenna is realized by substrate-integrated waveguide (SIW) on low-temperature cofired ceramic (LTCC). Due to low profile, light weight, and readiness for both fabrication and integration, it can be seen that microstrip antennas are suitably employed for the 5G millimetre-wave systems. Series-fed structures are often used in many millimetre-wave patch array antennas [13–15], especially for the systems in the 37/39-GHz band, because

Table 1: Comparison of reference.

Ref	elements	f_0,(GHz)	BW,(%)	SLL,(dB)	Scan	EIRP,(dB)
[7]	8	28	4.7			
[9]	8	21.5	3.2		±40°	
[10]	8	28/38	5		±20°	
[16]	5	5	2.4			
[17]	48	60	2.5	7	±32°	
[20]	64	28		13	±30°	37
[21]	32	29	21		±50°	41
This work	64	37.5	8	25	±40°	48

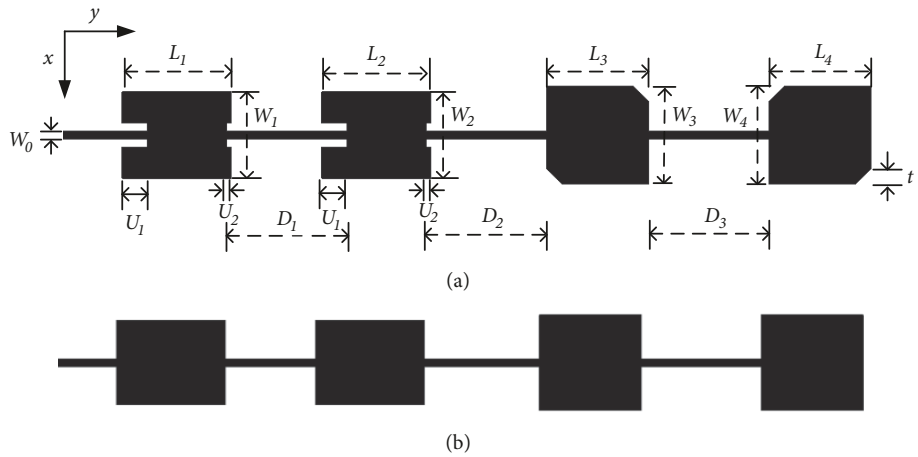

Figure 1: (a) The proposed and (b) the conventional series-fed array of microstrip patches.

the less complexity of the feeding circuits is preferred for the antenna gain enhancement. From the comparison in Table 1 [7, 9, 10, 16, 17], it can be seen that the impedance bandwidths of the series-fed antenna arrays range from 2.4% to 5%. The bandwidth of microstrip antenna on a thin laminate tends to be narrow, often less than 3% [18, 19]. For the band from 37 to 38.6 GHz, the bandwidth is required to be at least 4.3% [6]. A multitude of structures may be used to increase the bandwidth of microstrip antenna, for example, stacked patches [19]. However, the structure complexity can often lead to extra loss.

Base station antennas are generally required to have high gain, beam steering, or multibeam capability for multi-frequency applications. Active electronically scanned arrays (AESAs) are a promising technology to address the 5G base station antenna design. AESAs can shift the beam with agility while exhibiting real-time beam control, low side-lobe, high gain, wide scan angle, wide bandwidth, and MIMO capabilities [20, 21]. A comparison of the important parameters such as frequency, number of elements, bandwidth (BW), side-lobe level (SLL), scan coverage, and effective isotropic radiated power (EIRP) has been summarized in Table 1.

The focus of the paper is on developing a 37/39GHz active phased array with the beamforming capability in the azimuthal direction. In the vertical direction, the patches are combined by a series-fed configuration which yields a fixed beam shape in the elevation direction. Also, the return loss bandwidth of the array will be more than 8%. The outline of this paper is as follows. Section 2 describes the modified series-fed patch antenna featuring improved bandwidth and low loss. The procedure to increase the bandwidth is given and demonstrated by a series-fed antenna with four patches. The formation of a 16-element array based on the designed four-patch array is addressed. The weighting coefficients required in the beamforming system are also discussed. In Section 3, the simulation and experiment results are presented and compared. Finally, a conclusion is given in Section 4.

2. Antenna Array Design

2.1. Bandwidth-Enhanced Series-Fed Microstrip Patches. The proposed and the conventional series-fed array of microstrip patches are illustrated in Figures 1(a) and 1(b), respectively. In the figure, four resonant patches are connected using a single straight transmission line. The frequency response of the input impedance of a single patch is simulated and shown in Figure 2. When the patch is not perturbed as in Figure 1(b), one resonance is observed at 37.4 GHz. If the opposite corners are truncated as in Figure 1(a), the resonance splits into two degenerate modes [18, 22]. A patch on the Duroid 5880 substrate with $\varepsilon_r = 2.2$, h (thickness)=10 mil, $W_4 = 2.5$ mm, and $L_4 = 2.56$ mm is designed and simulated. It can be shown in Figure 2 that larger truncation (t) leads to more

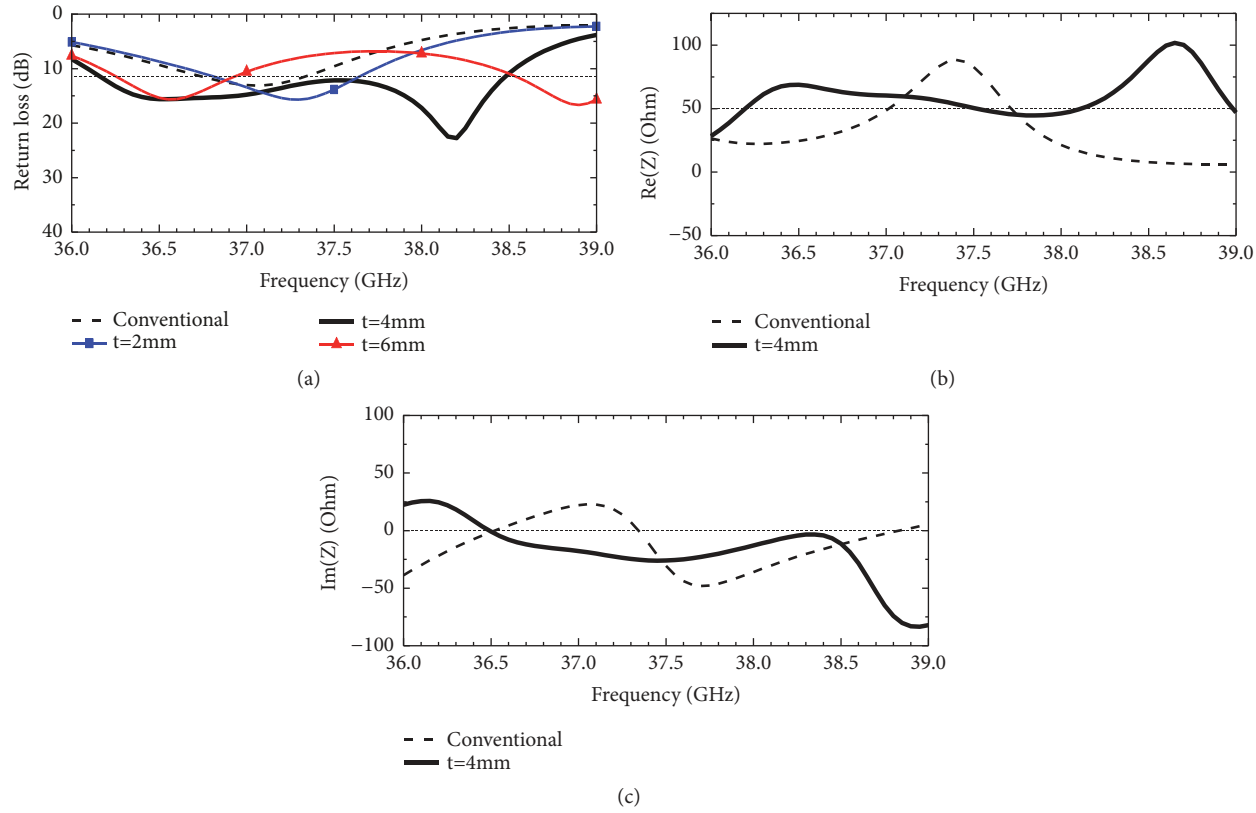

FIGURE 2: Simulated performances of the truncated patch antennas. (a) Return loss, (b) Re(Z), and (c) Im(Z).

mode separation and wider bandwidth. The radiated fields excited by these two modes, which are perpendicular to each other, are not linearly polarized. Nevertheless, pure linear polarization can be achieved when left-handed and right-handed elliptical polarizations are adequately combined [23].

As shown in Figure 1(a), the two patches at the end of the array are arranged to produce y-directed linear polarization and retain the enhanced bandwidth. The formation of the array can be designed to further lessen the cross-polarization radiation, which will be discussed later. The width of the patch may be varied to achieve the desired radiation conductance [24–28]. To build a linear array with beamforming capability, however, the patch width has to be limited to less than the element spacing, usually $\lambda/2$, to avoid the unwanted mutual coupling between patches due to proximity. The input impedance of the edge-fed patch can be adjusted by using an inset feed recessed a distance from the edge [16]. Furthermore, at the first patch, a quarter-wavelength transformer can be employed as the feed line which can ease the realization of the required input impedance.

When the width of the connecting line is fixed, $W_0 = 0.2$ mm, the dimensions of the series-fed patches are U_1 =0.63, U_2 =0.12, $L_1 = 2.74$, $L_2 = 2.74$, $L_3 = 2.56$, $L_4 = 2.56$, $W_1 = 2.2$, $W_2 = 2.2$, $W_3 = 2.5$, $W_4 = 2.5$, $t = 0.4$, and $D_1 = D_2 = D_3 = 3$, all in mm. The simulated values of the input impedance of the patches are given as follows: $Z_1 = 150.8$, $Z_2 = 150.8$, $Z_3 = 262.5$, and $Z_4 = 262.7$ohm, respectively.

Figure 2(a) shows that 6.6% bandwidth can be achieved for the corner-truncated patch compared to only 2.6% bandwidth for the rectangular one, if 10-dB return loss is specified. At resonance of 38.2GHz as shown in Figures 2(b) and 2(c), the real part of the input impedance is 54.6 ohm and the image part of the input impedance is -3.4 ohm, which is approximately matched to the input impedance $Z_0 = 50$ ohm.

The layouts of four kinds of series-fed antennas are illustrated in Figure 3. The transmission line between two adjacent patches is of about one half-wavelength ($D_0 = 4$mm). For layouts (a) and (b) as shown in Figure 3, an inset feed is used for the first patch. The width and the depth of the symmetrical rectangular notches can be tuned for impedance matching. Figure 4 shows that 6.6% bandwidth can be achieved for layout (a) compared to only 1.7% bandwidth for layout (b), if 10-dB return loss is specified. Without the inset for the first patch, layouts (c) and (d) cannot achieve 10-dB return loss requirement because of high input impedance.

The simulated H-plane and E-plane radiation patterns are plotted in Figures 5(a) and 5(b), respectively. It can be seen that the antenna gain can be at least 10 dBi with the first sidelobe suppression more than 13 dB. The H-plane cross-pol isolation, however, is only 10 dB. The cross-pol performance can be improved by the array formation described in Section 2.2.

2.2. Array Design to Reduce Cross-Polarization. In the formation of a linear array based on the proposed series-fed patch

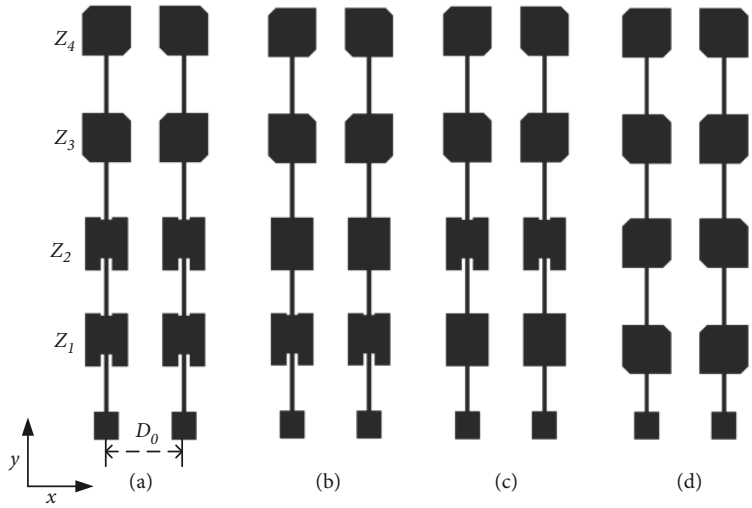

FIGURE 3: The layouts of four kinds of series-fed antennas (a)~(d) with the left-handed and the right-handed elliptical polarization types.

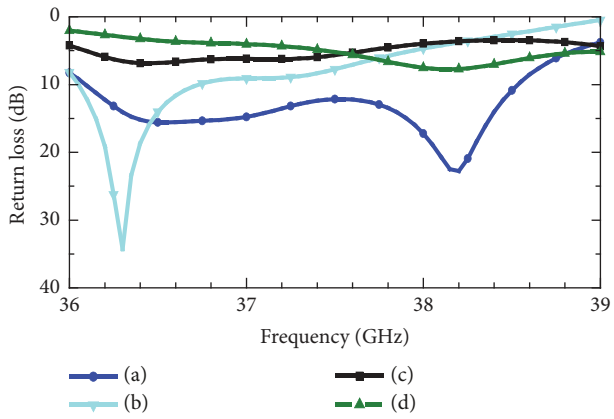

FIGURE 4: Series feed layout (a)~(d) return loss simulation.

antennas, left-handed and right-handed elliptical polarization patches are alternately used, as shown in Figure 3(a), for further reducing the cross-polarization radiation. For these two elliptical polarization types, the electric field can be, in general, respectively, expressed as

$$\vec{E} = E_0\left(j\alpha\vec{a}_x + \vec{a}_y\right) \tag{1a}$$

$$\vec{E} = E_0\left(-j\alpha\vec{a}_x + \vec{a}_y\right) \tag{1b}$$

where α can be regarded as the residual axial ratio, $|\vec{E_x}|/|\vec{E_y}|$, for a single series-fed antenna. Figure 6 shows the geometrical layout of a linear array with even number of elements. The array factor can be expressed as [29]

$$\sum_{n=1}^{N} a_n \vec{E}_n e^{j(2\pi/\lambda)x_n \sin(\theta_a - \theta_a')} \tag{2}$$

where a_n, E_n, and θ'_a denote the complex weighting, element pattern, and the beam direction, respectively. If N is even, the pattern can be shown to be

$$\sum_{n=1}^{N/2} 2\left(a_n\vec{E}_n + a_{N+1-n}\vec{E}_{N+1-n}\right)\cos\left[\frac{2\pi}{\lambda}\left(\frac{N+1}{2} - n\right)d\sin\left(\theta_a - \theta_a'\right)\right] \tag{3}$$

where d is the element spacing. The x-directional electric fields of the n-th and $(N+1-n)$-th elements can cancel with each other if the elliptical polarization types are different and the following condition is satisfied:

$$a_n = a_{N+1-n} \tag{4}$$

The cross-polarization radiation can be therefore reduced in the main beam direction. The condition of (4) for amplitude weightings can be readily achieved in various beamforming applications, for example, the well-known Taylor and Bayliss beams [29, 30]. It is noted that the azimuthal pattern is symmetric in theory when (4) is applied. Figure 7 shows the simulated H-plane and E-plane patterns of the 4×2 series-fed antennas, that is, $n = 2$. In Figure 7, it can be seen that the cross-polarization radiation is insignificant.

3. Beamforming Simulation and Experiment Results

Figure 8 shows the photograph of the fabricated 4×16 array based on the proposed series-fed patch antennas with the spacing $dx = 4$ mm. For accommodating transmit/receive module (TRM) to be installed from behind, an additional section of 50-ohm microstrip line, 4.47 mm in length, is alternately employed to connect the array and the probe feed. This extra microstrip line is compensated by the TRM, which integrates millimeter-wave components including a power amplifier (PA), a low-noise amplifier (LNA), an attenuator, a phase shifter, and switches. The least significant bits (LSB) of the phase shifter and the attenuator correspond to 11.25° and 1 dB, respectively.

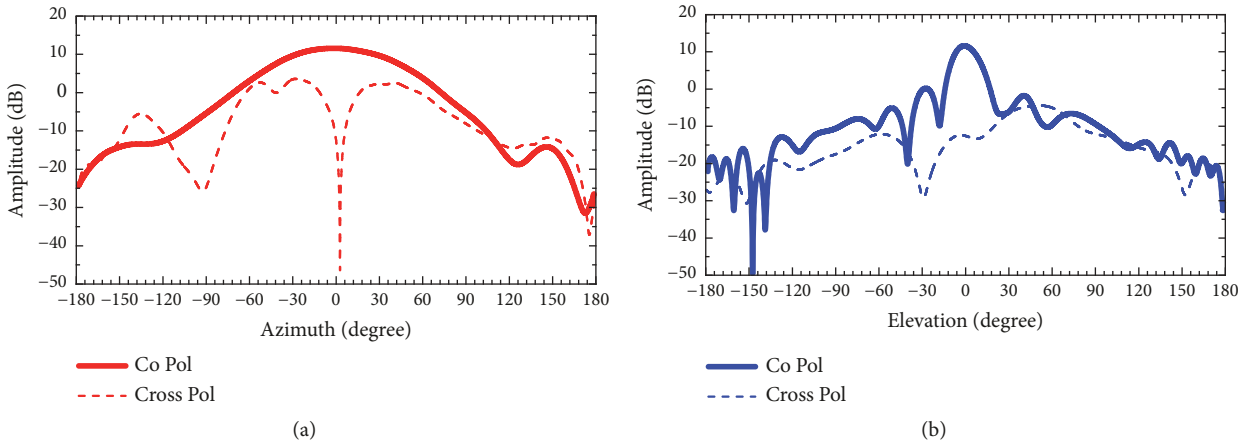

Figure 5: Simulated co-pol and cross-pol patterns of the proposed 4×1 series-fed antenna: (a) H-plane and (b) E-plane.

Table 2: The bit steps of the TR modules for the gains and phases.

Control state	Attenuator @38GHz	Phase shifter @38GHz	Transmit gain @38GHz	Receive gain @38GHz
00000	0	70.43	27.1	23.4
00001	-1.13	60.04	25.97	22.27
00010	-1.88	45.82	25.22	21.52
00100	-3.65	24.37	23.45	19.75
01000	-7.24	-20.22	19.86	16.16
10000	-14.82	-113.8	12.28	8.58
11111	-30.21	79.41	-3.11	-6.81

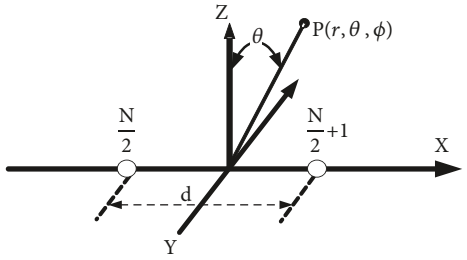

Figure 6: The geometrical layout of a linear array with even number of elements.

Each series-fed patch array is connected to a TR module through K type semirigid cable assembly, as shown in Figure 9. Figure 10 shows the feeding network of the array. In this network, a WR28 2-way power combiner is used to connect two WR28 8-way power combiners each of which connects eight TR modules.

The T/R modules fabricated by Transcom, as shown in Figure 11, are designed for the active phased array application. Power amplifiers are used to achieve the output power up to 0.5W. The noise figure of the low-noise amplifier (LNA) is less than 6.8dB. The 5-bit HMC939 attenuator and the 5-bit TGP2102 phase shifter are employed to adjust the amplitude and the phase with 1dB and 11.25° resolution, respectively. They are located in the common arm of transmit and receive path. A digital compensation algorithm is applied to increase the phase accuracy within ±5.625° and the amplitude accuracy within ±0.5dB. These algorithms are implemented by FPGA and flash memory with a lookup table. The transmitter P1dB and the receiver gain are 27.1dBm and 23.4dB, respectively. The typical values for gain and phase are shown in Table 2.

The probe feed of 15-mil in length is the pin extended from the center of a 50-ohm coaxial structure integrated with the back-plate. This configuration results in good isolation between TRM and antennas which, in turn, avoid affecting the radiation pattern. The measured return losses are shown in Figure 12(a) for the 1st, 7th, 8th, and 16th elements in Figure 8 which are located at the border and the middle of the array. These four elements exhibit the effects of different degrees of mutual coupling from the adjacent elements. The return losses are below -10 dB from 36 to 39 GHz. It is observed that the measured bandwidth can be slightly more than 8%. Figure 12(b) shows the experiment results of the isolation between the adjacent elements, which are at least 20dB.

In the phased array, the uncorrelated amplitude and phase errors of each element caused by active devices and discontinuities can be corrected by near-field alignment [31]. In this measurement procedure, an iterative process is developed to optimally set the states of the 5-bit phase shifters

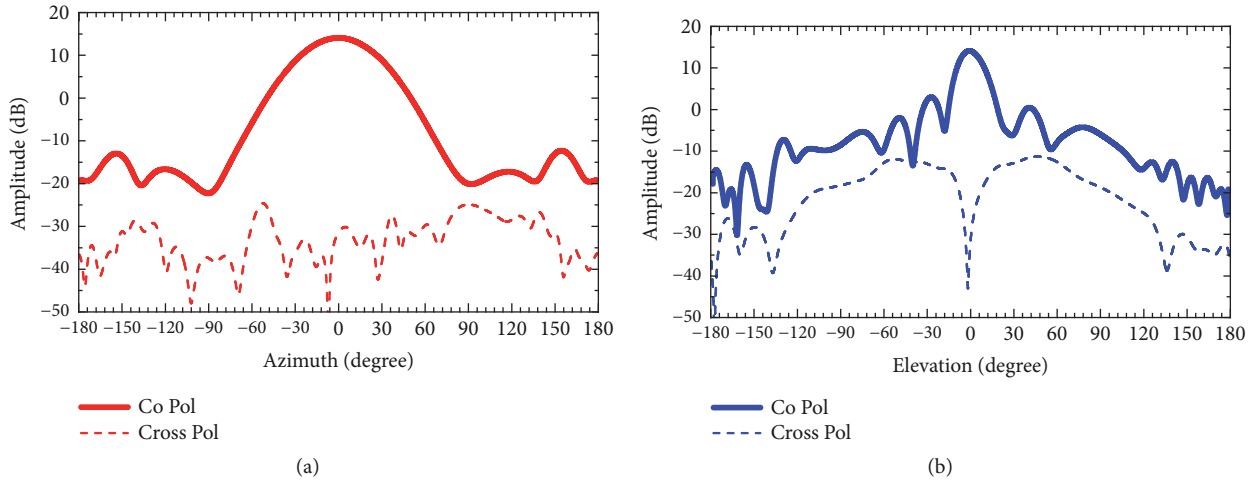

Figure 7: Simulated antenna patterns of the proposed 4×2 series-fed array antennas with reduced cross-polarization: (a) H-plane and (b) E-plane.

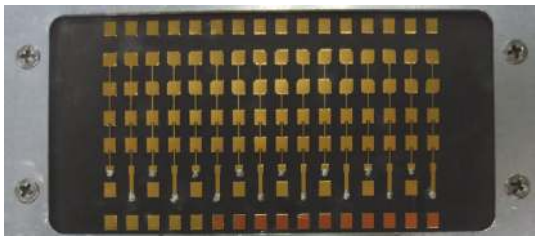

Figure 8: The photograph of the fabricated 4×16 array.

Figure 9: The connection of antennas and TR modules.

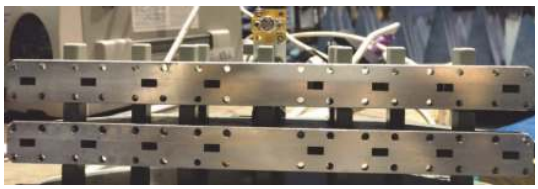

Figure 10: The photograph of the fabricated power combiner.

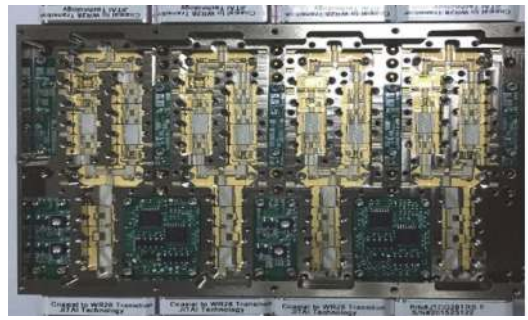

(a)

(b)

Figure 11: The photographs of the Transcom T/R modules (a) top view, (b) side view.

and attenuators until the measured gain and phase of each antenna can converge within ±0.5 dB and ±5.625°, respectively. Figures 13(a) and 14(a) present the measurements of the antenna patterns of the aligned 4×16 array with the uniform and low-sidelobe distributions, respectively. For the pattern with low sidelobes, the weighting coefficients are assigned to −13, −14, −6, −5, −3, −1, −1, 0, 0, −1, −1, −3, −5, −6, −14, and −13 dB for n = 1~16. It is noted that the E-plane patterns shown in Figures 13(b) and 14(b) exhibit a similar performance.

Figures 15(a) and 16(a) present the simulated and the measured results of the transmitting patterns with the uniform distribution for 37.6 GHz with beam steering along horizontal

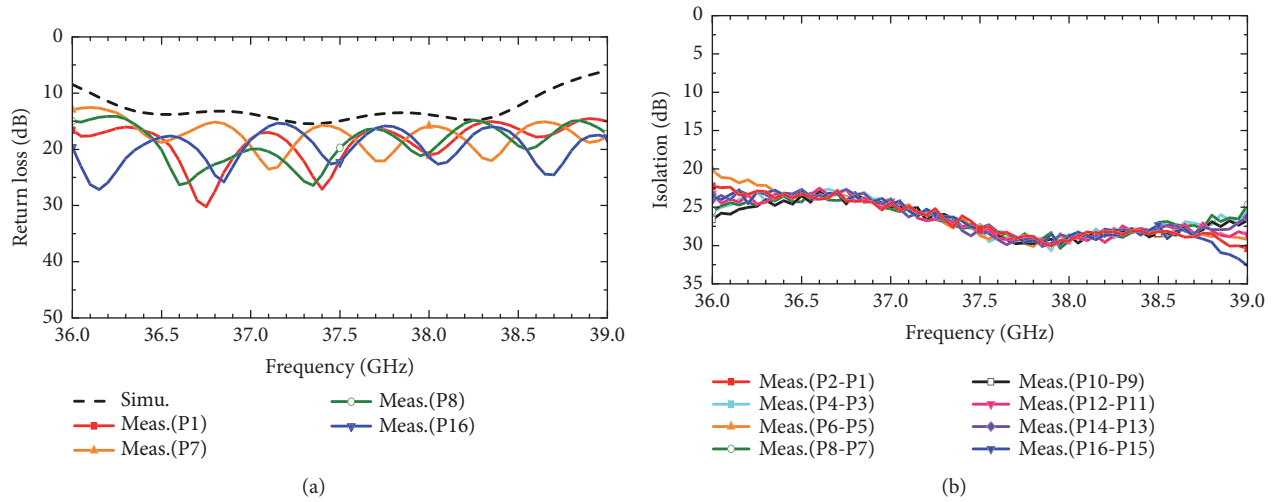

FIGURE 12: Measured and simulated antenna performances of the 4×16 series-fed array antennas: (a) return loss and (b) isolation.

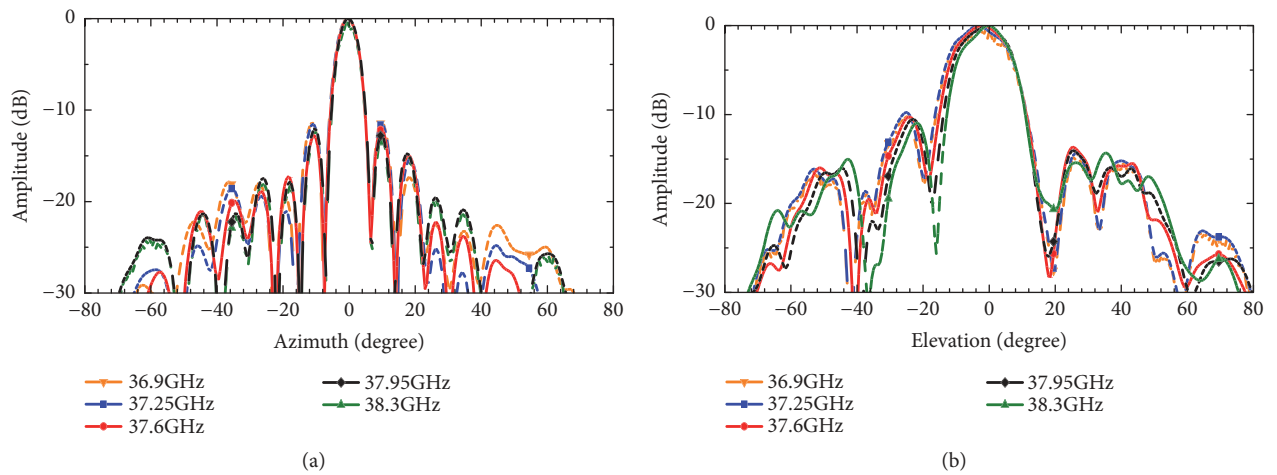

FIGURE 13: The measurement of the transmitting pattern of the aligned 4×16 array with the uniform distribution: (a) H-plane and (b) E-plane.

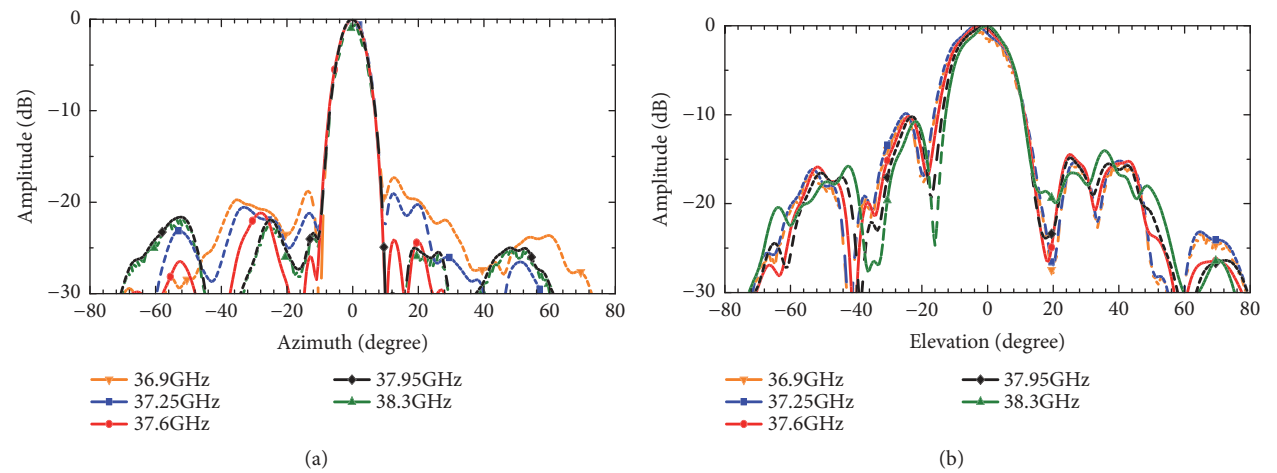

FIGURE 14: The measurement of the receiving pattern of the aligned 4×16 array with low sidelobes: (a) H-plane and (b) E-plane.

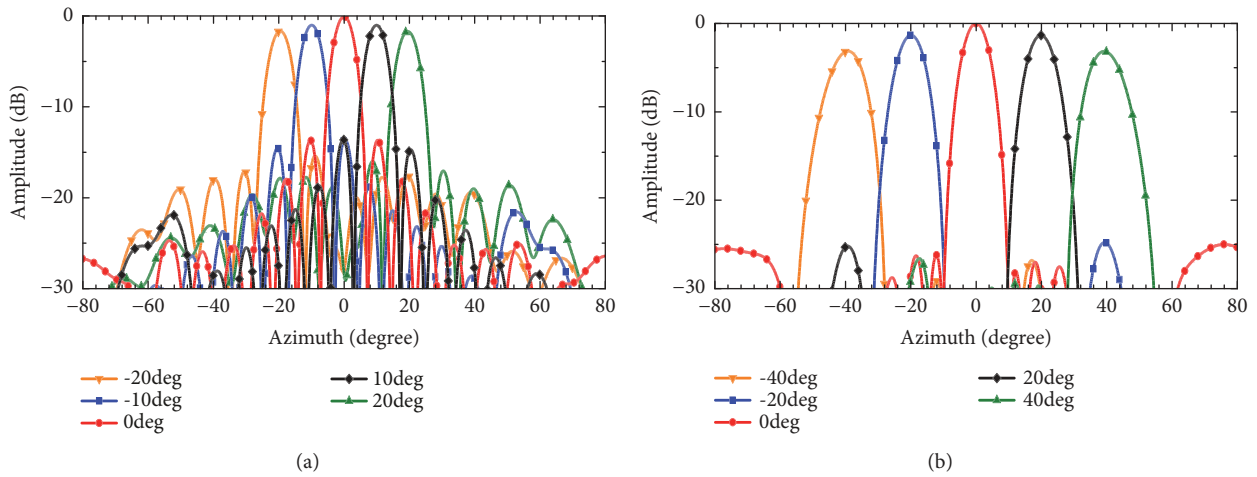

FIGURE 15: The simulation of the scanned H-plane patterns: (a) transmitting patterns with uniform distribution and (b) receiving patterns with low sidelobes.

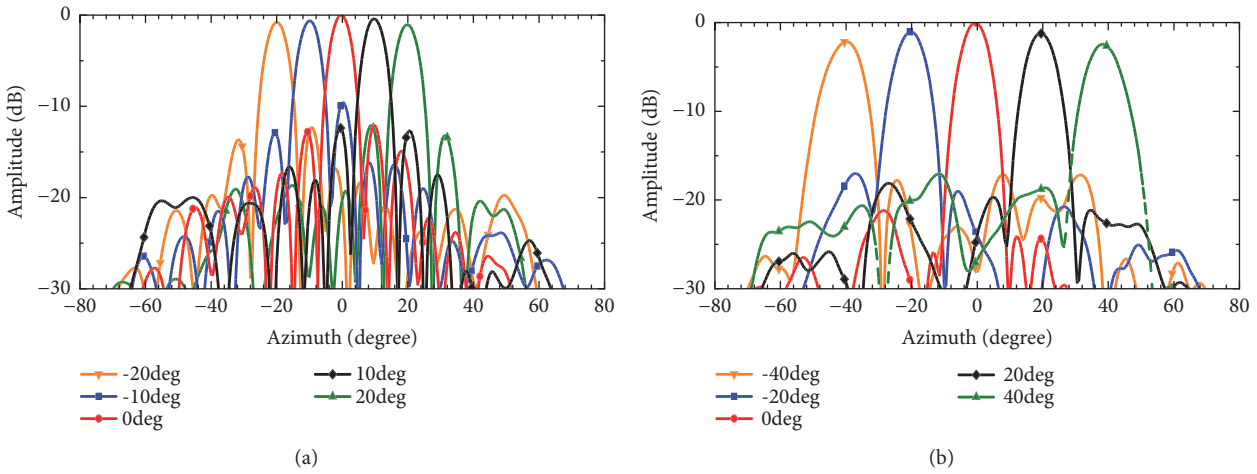

FIGURE 16: The measurements of the scanned H-plane patterns: (a) transmitting patterns with uniform distribution and (b) receiving patterns with low sidelobes.

directions by every 10° in the range of ± 20°. The main beam of the boresight exhibits the beamwidth of 5.5° while the first sidelobe rejection is approximately –13 dB. When the main beam scans to ±20°, the beamwidth becomes 6.5° and the scan loss is about 1 dB. Figures 15(b) and 16(b) present the simulation and measurement of the receiving patterns for 37.6 GHz with beam steering along horizontal directions by every 20°. The main beam of the boresight exhibits the beamwidth of 7.9° with 25 dB sidelobe rejection. When the main beam scans to ± 40°, the beamwidth becomes 10° and the scan loss is about 2.1dB. The sidelobe rejection is only 18 dB mainly due to the induced variations of the active devices in TRM.

Figures 17(a) and 17(b) show the H-plane and E-plane cross-polarization for the antenna with low-sidelobe weightings. In both cases, it can be seen that the cross-polarization is generally less than -20 dB. It is found that the rectangular patches arranged on the peripheral of the array antenna can reduce the cross-polarization radiation.

The measured gain curve of the 4×16 array is in agreement with the predicted gain obtained from the HFSS simulation as shown in Figure 18. The measured gain of array is approximately 21~22 dBi after the near-field alignment is achieved. It can be seen that the measured receiver gain stays fairly constant from 37 to 39 GHz.

4. Conclusion

In the paper, a novel configuration of microstrip series-fed patch array has been designed to enhance the bandwidth. Compared with the conventional one, this novel configuration has been verified to have a 21-dBi gain for 8% bandwidth by experiment. The proposed antenna can be used for 37/39 bands which is under the consideration for 5G applications. A 4 × 16 planar array has been prototyped and shown to exhibit good radiation characteristics in beam steering and sidelobe suppression. This active antenna offering high gain, good

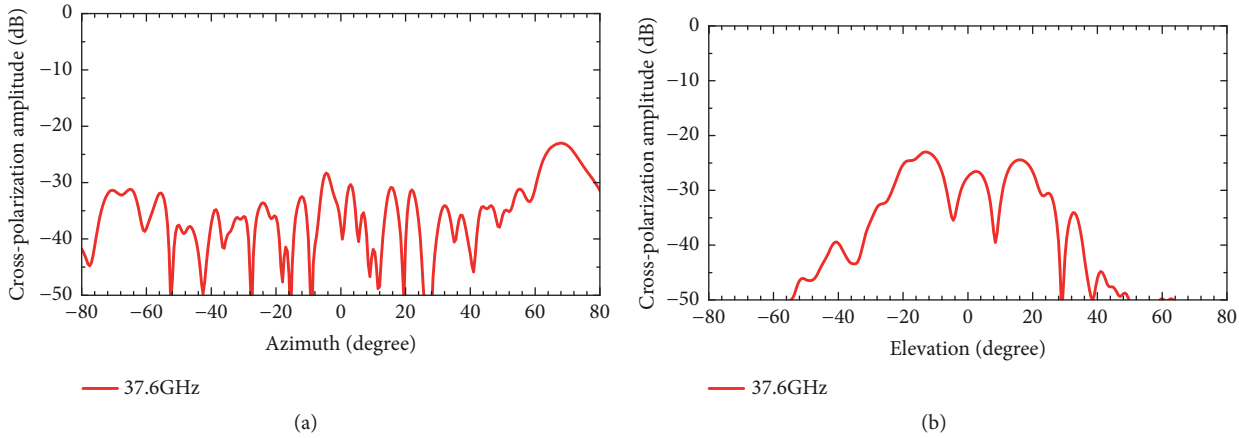

Figure 17: The measured cross-polarization of the antenna with low-sidelobe weightings: (a) H-plane and (b) E-plane.

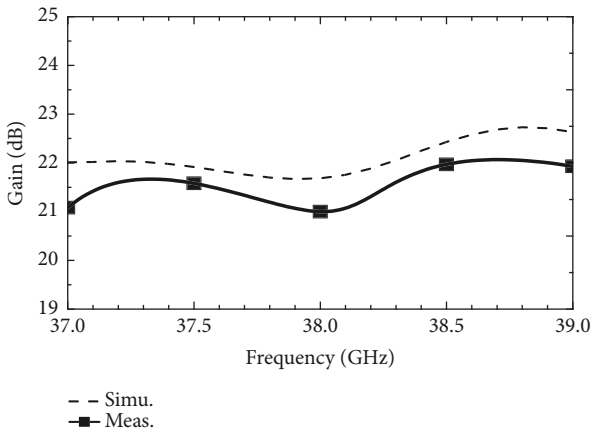

Figure 18: The measured and simulated gain curves of the 4×16 array in the broadside direction.

cross-polarization isolation, and flexible radiation patterns is suitable for millimetre-wave beamforming applications.

Data Availability

The data used to support the findings of this study are included within the article.

Conflicts of Interest

The authors declare that there are no conflicts of interest regarding the publication of this paper.

Acknowledgments

This work was supported by the Ministry of Science and Technology, ROC, under grant MOST106-2221-E-008 -010.

References

[1] T. Rappaport, S. Sun, R. Mayzus et al., "Millimeter wave mobile communications for 5G cellular: it will work!," *IEEE Access*, vol. 1, pp. 335–349, 2013.

[2] W. Roh, J.-Y. Seol, J. Park et al., "Millimeter-wave beamforming as an enabling technology for 5G cellular communications: theoretical feasibility and prototype results," *IEEE Communications Magazine*, vol. 52, no. 2, pp. 106–113, 2014.

[3] A. Ghosh, T. A. Thomas, M. C. Cudak et al., "Millimeter-wave enhanced local area systems: a high-data-rate approach for future wireless networks," *IEEE Journal on Selected Areas in Communications*, vol. 32, no. 6, pp. 1152–1163, 2014.

[4] Z. Pi, J. Choi, and R. W. Heath, "Millimeter-wave Gbps broadband evolution towards 5G: Fixed access and backhaul," *IEEE Communications Magazine*, vol. 54, no. 4, pp. 138–144, 2016.

[5] Resolution 238, "Studies on frequency-related matters for International Mobile Telecommunications identification including possible additional allocations to the mobile services on a primary basis in portions of the frequency range between 24.25 and 86 GHz for the future development of IMT for 2020 and beyond," ITU, WRC-15, 2015.

[6] FCC, "Use of spectrum bands above 24 GHz for mobile radio," 2015.

[7] H. Zhou and F. Aryanfar, "A Ka-Band patch antenna array with improved circular polarization," in *Proceedings of the 2013 IEEE International Symposium on Antennas and Propagation & USNC/URSI National Radio Science Meeting*, pp. 225-226, Orlando, FL, USA, July 2013.

[8] W. Hong, K. Baek, . Youngju Lee, and . Yoon Geon Kim, "Design and analysis of a low-profile 28 GHz beam steering antenna solution for Future 5G cellular applications," in *Proceedings of the 2014 IEEE/MTT-S International Microwave Symposium - MTT 2014*, pp. 1–4, Tampa, FL, USA, June 2014.

[9] N. Ojaroudiparchin, M. Shen, S. Zhang, and G. F. Pedersen, "A switchable 3-D-coverage-phased array antenna package for 5G mobile terminals," *IEEE Antennas and Wireless Propagation Letters*, vol. 15, no. 11, pp. 1747–1750, 2016.

[10] M. M. Ali and A. R. Sebak, "Design of compact millimeter wave massive MIMO dual-band (28/38 GHz) antenna array for future 5G communication systems," in *Proceedings of the 2016 17th International Symposium on Antenna Technology and*

Applied Electromagnetics (ANTEM), pp. 1–4, Montreal, Canada, July 2016.

[11] M. Khalily, R. Tafazolli, T. A. Rahman, and M. R. Kamarudin, "Design of phased arrays of series-fed patch antennas with reduced number of the controllers for 28-GHz mm-wave applications," *IEEE Antennas and Wireless Propagation Letters*, vol. 15, pp. 1305–1308, 2016.

[12] H. Chu and Y.-X. Guo, "A filtering dual-polarized antenna subarray targeting for base stations in millimeter-wave 5G wireless communications," *IEEE Transactions on Components, Packaging, and Manufacturing Technology*, vol. 7, no. 6, pp. 964–973, 2017.

[13] T.-Y. Han, "Series-Fed Microstrip Array Antenna with Circular Polarization," *International Journal of Antennas and Propagation*, vol. 2012, Article ID 681431, 5 pages, 2012.

[14] B. H. Ku, P. Schmalenber, O. Inac et al., "'A 77–81 16-element phased-array receiver with $\pm 50^o$ beam scanning for advanced automotive radar," *IEEE Transactions on Microwave Theory and Techniques*, vol. 62, no. 11, pp. 2823–2832, 2014.

[15] S. Krishna, G. Mishra, and S. K. Sharma, "A series fed planar microstrip patch array antenna with 1D beam steering for 5G spectrum massive MIMO applications," in *Proceedings of the 2018 IEEE Radio and Wireless Symposium (RWS)*, pp. 209–212, Anaheim, CA, January 2018.

[16] T. Yuan, N. Yuan, and L.-W. Li, "A novel series-fed taper antenna array design," *IEEE Antennas and Wireless Propagation Letters*, vol. 7, pp. 362–365, 2008.

[17] V. Semkin, F. Ferrero, A. Bisognin et al., "Beam switching conformal antenna array for mm-wave communications," *IEEE Antennas and Wireless Propagation Letters*, vol. 15, pp. 28–31, 2016.

[18] K. R. Carver and J. W. Mink, "Microstrip antenna technology," *IEEE Transactions on Antennas and Propagation*, vol. 29, no. 1, pp. 2–24, 1981.

[19] J. R. James and P. S. Hall, "Handbook of microstrip antenna," in '*Handbook of microstrip antenna*', p. chap, Peter Peregrinus, 1989.

[20] B. Sadhu, Y. Tousi, J. Hallin et al., "A 28GHz 32-element phased-array transceiver IC with concurrent dual polarized beams and 1.4 degree beam-steering resolution for 5G communication," in *Proceedings of the 2017 IEEE International Solid- State Circuits Conference - (ISSCC)*, pp. 128-129, San Francisco, CA, USA, Feburary 2017.

[21] K. Kibaroglu, M. Sayginer, and G. M. Rebeiz, "An ultra low-cost 32-element 28 GHz phased-array transceiver with 41 dBm EIRP and 1.0-1.6 Gbps 16-QAM link at 300 meters," in *Proceedings of the 2017 IEEE Radio Frequency Integrated Circuits Symposium, RFIC 2017*, pp. 73–76, USA, June 2017.

[22] M. Haneishi, T. Nambara, and S. Yoshida, "Study on ellipticity properties of single-feed-type circularly polarised microstrip antennas," *IEEE Electronics Letters*, vol. 18, no. 5, pp. 191–193, 1982.

[23] S. Gao, Q. Luo, and F. Zhu, *Circularly Polarized Antenna*, John Wiley & Sons, 2014.

[24] A. G. Derneryd, "Linearly polarized microstrip antennas," *IEEE Transactions on Antennas and Propagation*, vol. 24, no. 6, pp. 846–851, 1976.

[25] T. Metzler, "Microstrip series arrays," *IEEE Transactions on Antennas and Propagation*, vol. 29, no. 1, pp. 174–178, 1981.

[26] B. B. Jones, F. Y. M. Chow, and A. W. Seeto, "The synthesis of shaped patterns with series-fed microstrip patch arrays," *IEEE Transactions on Antennas and Propagation*, vol. 30, no. 6, pp. 1206–1212, 1982.

[27] D. G. Babas and J. N. Sahalos, "Synthesis method of series-fed microstrip antenna arrays," *IEEE Electronics Letters*, vol. 43, no. 2, pp. 78–80, 2007.

[28] S. Sengupta, D. R. Jackson, and S. A. Long, "A method for analyzing a linear series-fed rectangular microstrip antenna array," *Institute of Electrical and Electronics Engineers. Transactions on Antennas and Propagation*, vol. 63, no. 8, pp. 3731–3736, 2015.

[29] R. J. Mailloux, *Phased Array Antenna Handbook*, Artech House, 2nd edition, 2005.

[30] H. J. Orchard, R. S. Elliott, and G. J. Stern, "Optimising the synthesis of shaped beam antenna patterns," *IEE Proceedings H - Microwaves, Antennas and Propagation*, vol. 132, no. 1, pp. 63–68, 1985.

[31] W. T. Patton and L. H. Yorinks, "Near-field alignment of phased-array antennas," *IEEE Transactions on Antennas and Propagation*, vol. 47, no. 3, pp. 584–591, 1999.